







# An improved setup for radial diffraction experiments at high pressures and high temperatures in a resistive graphite-heated diamond anvil cell

Cite as: Rev. Sci. Instrum. **91**, 045121 (2020); <https://doi.org/10.1063/1.5143293>

Submitted: 22 December 2019 . Accepted: 07 April 2020 . Published Online: 28 April 2020

J. Immoor , H. Marquardt , L. Miyagi , S. Speziale , S. Merkel , I. Schwark, A. Ehnes, and H.-P. Liermann 



View Online



Export Citation



CrossMark

Lock-in Amplifiers  
up to 600 MHz



Watch



# An improved setup for radial diffraction experiments at high pressures and high temperatures in a resistive graphite-heated diamond anvil cell

Cite as: Rev. Sci. Instrum. 91, 045121 (2020); doi: 10.1063/1.5143293

Submitted: 22 December 2019 • Accepted: 7 April 2020 •

Published Online: 28 April 2020



J. Immoor,<sup>1,a)</sup> H. Marquardt,<sup>2</sup> L. Miyagi,<sup>3</sup> S. Speziale,<sup>4</sup> S. Merkel,<sup>5</sup> I. Schwark,<sup>6</sup> A. Ehnes,<sup>6</sup> and H.-P. Liermann<sup>6</sup>

## AFFILIATIONS

<sup>1</sup>Bayerisches Geoinstitut BGI, University of Bayreuth, 95440 Bayreuth, Germany

<sup>2</sup>Department of Earth Sciences, University of Oxford, Oxford OX1 3AN, United Kingdom

<sup>3</sup>University of Utah, 115 So. 1460 E., Salt Lake City, Utah UT84112-0111, USA

<sup>4</sup>German Research Center for Geosciences GFZ, 14473 Potsdam, Germany

<sup>5</sup>Univ. Lille, CNRS, INRAE, Centrale Lille, UMR 8207 - UMET - Unité Matériaux et Transformations, F-59000 Lille, France

<sup>6</sup>Photon Sciences, Deutsches Elektronen-Synchrotron (DESY), 22607 Hamburg, Germany

<sup>a)</sup> Author to whom correspondence should be addressed: [Julia.immoor@uni-bayreuth.de](mailto:Julia.immoor@uni-bayreuth.de)

## ABSTRACT

We present an improved setup for the experimental study of deformation of solids at simultaneous high pressures and temperatures by radial x-ray diffraction. This technique employs a graphite resistive heated Mao–Bell type diamond anvil cell for radial x-ray diffraction in combination with a water-cooled vacuum chamber. The new chamber has been developed by the sample environment group at PETRA III and implemented at the Extreme Conditions Beamline P02.2 at PETRA III, DESY (Hamburg, Germany). We discuss applications of the new setup to study deformation of a variety of materials, including ferropericlase, calcium perovskite, bridgmanite, and tantalum carbide, at high-pressure/temperature.

Published under license by AIP Publishing. <https://doi.org/10.1063/1.5143293>

## I. INTRODUCTION

Understanding the physical and rheological properties of materials at simultaneous high pressures and temperatures is of key importance in Earth science as well as materials sciences. The rheological properties of Earth's mantle materials, for example, govern large-scale mantle convection.<sup>1–4</sup> In addition, Crystallographic Preferred Orientation (CPO) caused by the alignment of mantle minerals during deformation leads to seismic anisotropy, providing a means to link seismic observations to the mantle flow.<sup>5–13</sup> Several techniques have been developed in the past to study the rheology of materials under high pressure and temperature, but achievable pressures are mostly limited to those typical of the crust and upper mantle.<sup>3,14–18</sup>

Deformation experiments at deep lower mantle pressures are almost exclusively performed in diamond-anvil cells in combination with synchrotron-based *in situ* x-ray diffraction in a radial geometry [Figs. 1(a) and 1(b)]. By employing the radial diffraction geometry, lattice strains and deviatoric stress as well as evolution of CPO can be derived from the analysis of *in situ* diffraction images. Radial x-ray diffraction in DACs has been widely employed in Earth science as well as materials sciences, but high-pressure experiments have been mostly limited to room temperature.<sup>19–25</sup> Early high-temperatures studies employed a laser-heated diamond anvil cell (DAC), but data analysis and interpretation is challenging due to temperature gradients in the sample.<sup>26,27</sup> Liermann *et al.*<sup>28</sup> developed a resistive-heated DAC, which was tested up to 36 GPa and 1100 K while performing *in situ* radial x-ray

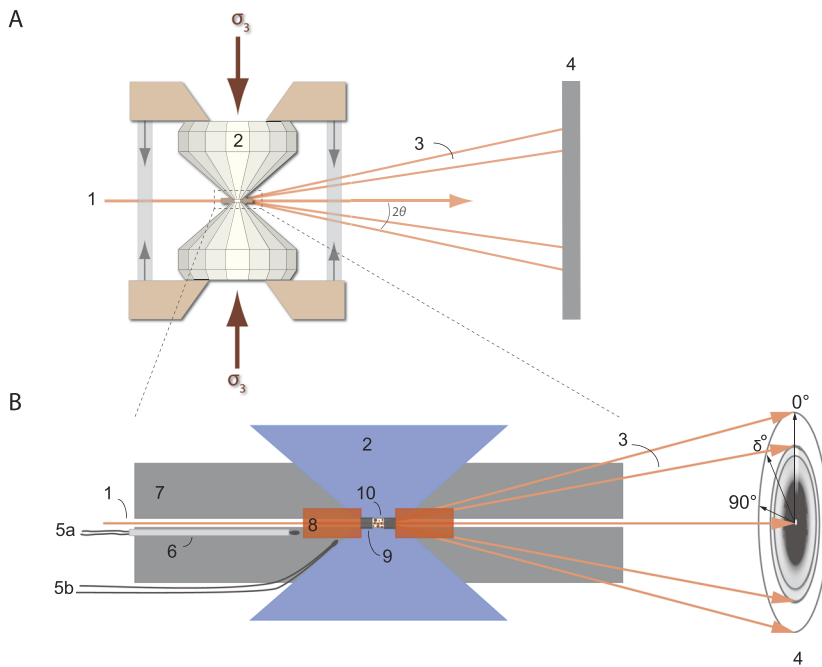


**FIG. 1.** (a) Angle-dispersive high-pressure radial x-ray diffraction in a DAC (modified after<sup>28</sup>),  $\sigma_3$ : stress along compression direction,  $2\theta$ : diffraction angle, 1: incoming x-ray beam, 2: diamond anvil, 3: diffracted beam, and 4: area detector. (b) Magnification of the diamond-anvil culets showing the position for the two thermocouples (5a: between both graphite heaters and 5b: on the diamond anvil next to the culet). 6: ceramic sleeve, 7: flexible graphite sheet, 8: Kapton, 9: boron gasket, and 10: sample.

diffraction. The use of a resistive-heating setup reduces temperature gradients and provides more homogeneous heating of the entire sample chamber.

Here, we present a modified resistive-heated-radial-x-ray-diffraction-diamond-anvil-cell (RH-rXRD-DAC) [Figs. 2(a) and 2(b)] and report on its performance during *in situ* radial x-ray diffraction experiments at simultaneous high pressure and high

temperature on several polycrystalline samples. The main improvement as compared to the setup described by Liermann *et al.* is the development and implementation of a water-cooled vacuum chamber [Figs. 3(a) and 3(b)] that also enables cooling of the piston of the Mao-Bell type DAC. This modification decreases heating and thermal expansion of the piston of the DAC but allows the cylinder to heat up, thus reducing friction between the piston and the

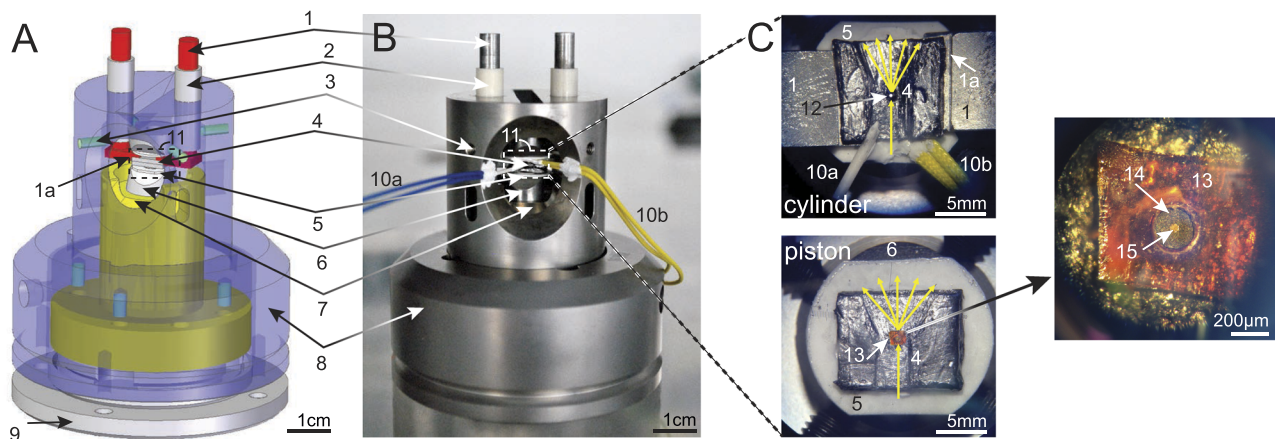


**FIG. 2.** Experimental setup of a resistive-heated DAC (modified after<sup>10</sup>). (a) 3D CAD model and (b) photograph of the resistive-heated DAC used for the experiments. 1: molybdenum rods (electrical contacts), 1a: strip with step at the end of the molybdenum rod, 2: ceramic sleeves, 3: screws, 4: graphite sheet, 5: ceramic plate, 6: tungsten carbide seat, 7: piston, 8: cylinder, 9: membrane cup (missing in B), 10a: thermocouple with ceramic sleeve, 10b: thermocouple, and 11: graphite-heater. (c) Close-up view of 11. Cylinder: 12—culet of a diamond and 4—flexible graphite sheet with carved space for the x-ray beam. The inset shows the lower diamond pressed into the graphite heater and illustrates the positions of the thermocouples. Piston: 13—Kapton, which supports a cubic boron nitride gasket or amorphous boron epoxy gasket (14) with powder sample in the sample chamber (15).

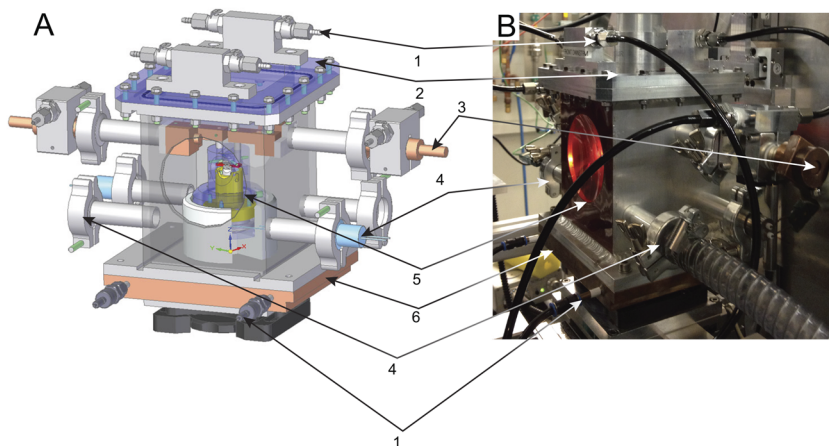


**FIG. 3.** (a) 3D CAD model of the vacuum chamber. (b) Photograph of the vacuum chamber while performing a high-temperature experiment ( $\sim 1400$  K). 1: water cooling inlet/outlet, 2: lid with screws, 3: power supply connector, 4: vacuum pump connection, 5: Kapton window, and 6: copper cooling plate.

cylinder during compression at high temperatures. The use of a vacuum chamber prevents the oxidation of the cell, the molybdenum rods, and the diamonds at very high temperatures. We discuss applications of the improved setup for studying the deformation behavior of major materials expected in Earth's lower mantle as well as tantalum carbide.

## II. EXPERIMENTAL METHOD

In radial x-ray diffraction experiments, the incoming x-ray beam is oriented perpendicular to the compression direction, i.e., the axis of the diamond anvils [Figs. 1(a) and 1(c): 1]. This setup provides the possibility to study the lattice strains, resulting from the effect of differential stress, together with the CPO of powder samples.<sup>19</sup> A pressure-transmitting medium is not used. This enhances the development of differential stress and texture. In order for x rays to reach the sample chamber in the radial diffraction geometry, x-ray transparent gaskets are required. Here, we used either x-ray transparent amorphous boron epoxy + kapton<sup>29</sup> or cubic boron nitride (cBN) epoxy<sup>27</sup> (10:1 Epotech 353ND) + kapton gaskets [Fig. 1: 8 and 9; Fig. 2(c): 13 and 14] to reach high pressures.<sup>30</sup> The culet sizes of the employed diamonds were  $200\text{ }\mu\text{m}$  or  $300\text{ }\mu\text{m}$  [Fig. 2(c): 12]. The setup of the graphite heater is similar on the piston and cylinder side of the DAC [Fig. 2(c)]. Diamonds are glued on tungsten carbide seats that are truncated at the side to increase the opening angle for diffracted x rays (Fig. 2: 5). The seats are insulated from graphite by a ceramic ring (Fig. 2: 4) fixed to the seat with OMEGABOND 500 liquid. The gaps between the ceramic plates and the diamonds are filled with ceramic glue (Resbond 989). The heads of the molybdenum rods end in horizontal strips with a small step at the end. A piece of graphite foil connects the molybdenum rods [Fig. 2(a): 1a, Fig. 2(b): 11, and Fig. 2(c): 1a] and serves as the heating element surrounding the diamond-anvils. A space is carved in the graphite foil to prevent diffraction of graphite contaminating the diffraction image. Two thermocouples (R-type) are attached to the cylinder side. One thermocouple is placed close to the tip of the diamond on the upstream side of the DAC and to the side of the path of the incident x-ray beam [Fig. 2(c): 10a]. The second thermocouple is positioned on

the graphite sheet, likewise upstream, and to the side of the incident x-ray beam [Fig. 2(c): 10b]. When the cell is closed, the second thermocouple rests between the graphite sheets of the piston and the cylinder.

During the experiment, the temperature of the sample can be increased/decreased by varying an analog I/O signal from 0 V to 10 V using the beamline control system. This proportionally adjusts the power of the DC power supply from 0 W to 1800 W (0–8 V and 0–220 A).<sup>31</sup> Pressure is changed remotely using a gas membrane device that is operated by using the membrane pressure controller APD200 from Sanchez Technology.<sup>27,28,32</sup>

For high-pressure and high-temperature experiments, the RH-rXRD-DAC is placed in a newly designed water-cooled vacuum chamber that serves to both cool the DAC and prevent oxidation of the DAC, the molybdenum electrodes, the diamond anvils, and the graphite heater [Figs. 3(a) and 3(b)]. The piston of the DAC is indirectly cooled through a steel pin that is connected to the base of the vacuum chamber, which is water-cooled. The differential cooling between the piston and the cylinder reduces the friction between the two parts of the DAC and enables a smoother pressure increase as compared to the previous experimental setup.<sup>27,28</sup> During the experiment, the vacuum in the chamber can be as good as  $5 \times 10^{-3}$  mbar. Note that, due to connections between the pump and the cell chamber, vacuum levels around the diamond anvil cells may not be as efficient. Nevertheless, the achieved vacuum is sufficient to perform experiments with minimal oxidation of the heating elements.

## III. RESULTS AND DISCUSSION

The new setup has been tested during different experimental campaigns at the Extreme Conditions Beamline (ECB) P02.2 at PETRA III, DESY (Hamburg, Germany). Diffraction images were collected with a XRD 1621 flat panel detector from Perkin Elmer. In the following, we will describe some selected experiments in order to illustrate the capability of the new setup for Earth and materials science research. We report on the deformation of polycrystalline samples of ferropericlasite [ $(\text{Mg}_{0.8}\text{Fe}_{0.2})\text{O}$ ], the *in situ* synthesis and deformation of cubic Ca-Pv ( $\text{CaSiO}_3$ ), experiments performed on



a two-phase mixture of bridgmanite ( $\text{MgSiO}_3$ ) and ferropericlasite, synthesized from a mixture of enstatite glass + ferropericlasite in the resistive-heated DAC, and the high-temperature compression of tantalum carbide ( $\text{TaC}_{0.99}$ ), an ultra-high temperature ceramic material.

### A. *In situ* deformation of ferropericlasite

Ferropericlasite is the second most abundant mineral in Earth's lower mantle. It may play a key role in mantle dynamics since it is rheologically weaker than bridgmanite, the dominant lower mantle phase. Furthermore, it shows a pronounced elastic anisotropy, making it one of the candidates to explain seismic shear wave polarization anisotropy in the lower mantle.<sup>33</sup> However, previous deformation studies at pressures of the lower mantle were limited to room temperature due to experimental complexity.<sup>19,21–23,34,35</sup> In the work of Immoor *et al.*, we used the described setup to measure the deformation of ferropericlasite to 62 GPa at 1400 K and to higher pressures but at lower temperature. In our 1400 K run, the pressure of the sample was increased up to 40 GPa at room temperature and, afterward, heated up to 1400 K. During heating, the pressure of the sample dropped to below 20 GPa. We increased the pressure again and reached 62 GPa when diamond failure stopped the experiment. During compression, we collected high quality diffraction images of ferropericlasite. Based on these results, we were able to monitor the evolution of CPO in ferropericlasite and confirm a change in the slip system activity at high temperature, as predicted by computations.<sup>10</sup>

### B. *In situ* synthesis and deformation of cubic $\text{CaSiO}_3$

$\text{CaSiO}_3$  perovskite is expected to be an important mineral in Earth's transition zone and lower mantle, where it is the third most abundant phase for a pyrolitic mantle composition.<sup>36</sup> In a deeply subducted oceanic slab,  $\text{CaSiO}_3$  perovskite may account for up to

25 Vol.% of the transformed basaltic crust<sup>37</sup> and will affect the bulk rheological properties of the lithospheric slab. According to a recent computational study,<sup>38</sup> the shear wave anisotropy of  $\text{CaSiO}_3$  perovskite is about 15%–30% at conditions of the lower mantle. A strong CPO of  $\text{CaSiO}_3$  perovskite may, therefore, contribute to seismic anisotropy observations, in particular, in the shallow lower mantle or lowermost transition zone, where the elastic anisotropy is strongest. A previous  $\text{CaSiO}_3$  perovskite study has been limited to 49 GPa under ambient conditions.<sup>23</sup> At these conditions, however,  $\text{CaSiO}_3$  perovskite forms a pseudo cubic structure, and the exact nature of the distortion is still under debate,<sup>39–42</sup> whereas at temperatures typical for the lower mantle, the structure is cubic ( $Pm\bar{3}m$ )<sup>40–43</sup> and may show a different rheological behavior.  $\text{CaSiO}_3$  perovskite can be experimentally synthesized from  $\text{CaSiO}_3$  wollastonite at pressures of about 20 GPa and temperatures of about 1300 K<sup>44</sup> but is not quenchable under ambient conditions. This implies that studies of the physical properties of  $\text{CaSiO}_3$  perovskite need to be performed *in situ* and in the same pressure device where it has been synthesized.

Using the improved RH-rXRD-DAC, we were able to synthesize  $\text{CaSiO}_3$  perovskite and performed several successful deformation experiments reaching temperatures of up to 1500 K at pressures of 45 GPa. The starting material was amorphous  $\text{CaSiO}_3$  mixed with platinum powder as the pressure standard. Figure 4 shows two diffraction images collected during a compression experiment that reached a final pressure of 40 GPa at 1300 K. Cubic  $\text{CaSiO}_3$  perovskite was synthesized after increasing the temperature to 1300 K at which point the pressure dropped from 33 GPa to 27 GPa as a result of the phase transition [Fig. 4(b)]. The collected diffraction patterns show smooth diffraction rings, indicating a relatively small and homogeneous grain size of the synthesized cubic  $\text{CaSiO}_3$  perovskite. The large pressure drop at the transition also caused strain heterogeneity in Pt finely mixed with the sample [see Pt peaks asymmetry in Fig. 4(b)].

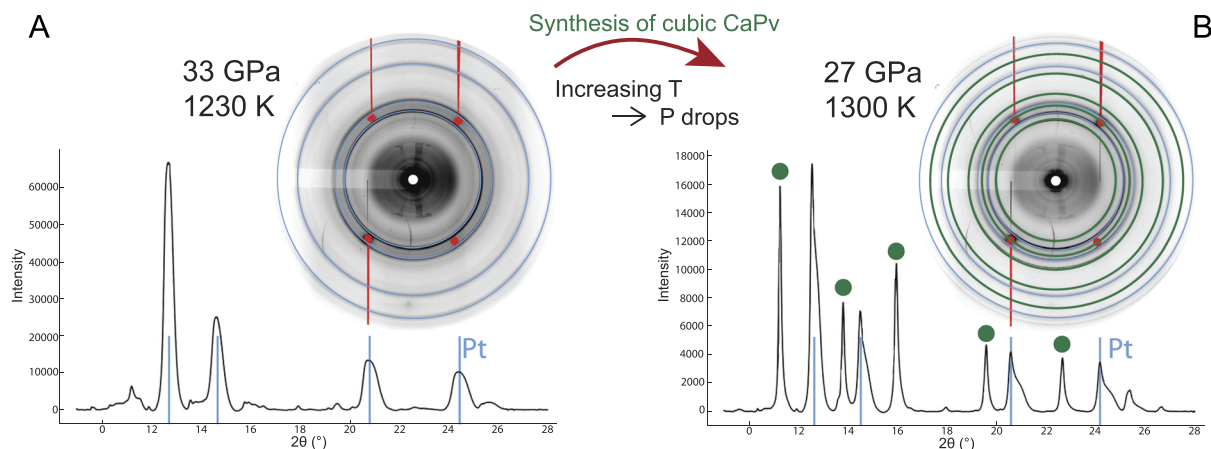


**FIG. 4.** Synthesis of cubic calcium perovskite. The pressure was calculated from the stronger Pt peak. (a) X-ray diffraction image at 33 GPa and 1230 K shows rings of Pt (blue), which are used to estimate the pressure during the experiment and diamond single-crystal diffraction spots (red). The corresponding integrated diffraction pattern is shown below with blue line indicating Pt peaks. (b) X-ray diffraction image at 27 GPa and 1300 K with Debye rings of Pt (blue), Debye rings of calcium perovskite (green), and diamond diffraction spots (red). At the bottom, integrated diffraction pattern with blue lines indicating Pt peaks and green dots indicating calcium perovskite peaks. In both panel (a) and (b), the diffraction lines of diamond are masked in the integration and are absent in the diffraction patterns.

### C. Synthesis of bridgmanite and ferropericlas

The deformation behavior of multiphase rock assemblies might substantially differ from the behavior of single-phase assemblies, particularly if the phases show large differences in rheological properties.<sup>35,45–48</sup> The lower mantle can be modeled as a two-phase mixture of bridgmanite and ferropericlas, two phases that show large differences in plastic strength and viscosity.<sup>3,5,22</sup> Because of this large contrast in rheological strength, it is difficult to predict mantle properties, including viscosity and seismic anisotropy, from single-phase measurements. There have been few deformation experiments on analogues,<sup>49,50</sup> as well as on a true two-phase lower mantle mixture, at pressures and temperature of the very top of the lower mantle using a rational Drickamer apparatus.<sup>3</sup> Here, we used the improved RH-rXRD-DAC to synthesize a bridgmanite and ferropericlas assembly [Figs. 5(a) and 5(b)] from an enstatite glass powder mixed with ferropericlas and applied deviatoric stress to the two-phase mixture at high temperatures [Fig. 5(c)]. In one successful run, we first increased the pressure to 58 GPa and the temperature to 1600 K. Afterward, the pressure in the sample decreased while increasing the temperature continuously to 1900 K. A peak splitting of ferropericlas was observed, likely as a result of pressure gradients in the sample chamber, followed by the appearance of the typical diffraction ring triplet of the new phase bridgmanite. Bridgmanite grew, while the pressure continued to decrease when the thermocouples stopped working. During a subsequent decrease in voltage and, therefore, presumably in temperature (based on power–temperature relation; see Fig. 6), the pressure in the sample chamber increased again to 35 GPa, leading to deformation of the sample [Fig. 5(c)].

### D. Compression of tantalum carbide (TaC<sub>0.99</sub>)

Carbides are characterized by high mechanical and thermal stability and play an important role in industrial applications, where they are used, for example, as coatings for abrasive tools. Many experimental and computational studies have been conducted on tantalum carbide (see Ref. 51). However, no experiments have been performed to study the behavior of this phase under simultaneous high pressure, high temperature, and deviatoric stress. We performed two successful experimental deformation runs on

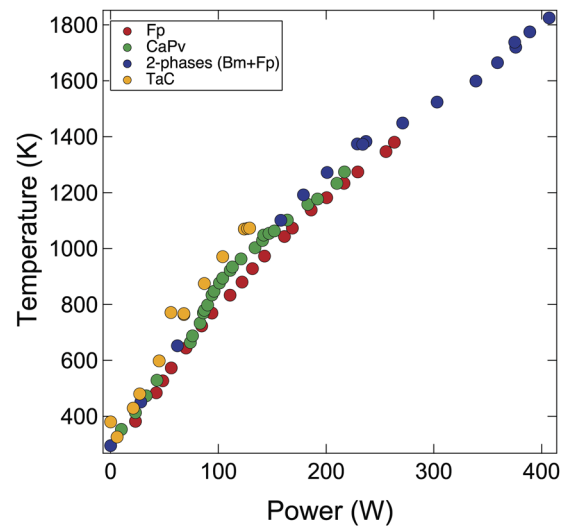


**FIG. 6.** Power–temperature curves of different experiments. Symbols: Fp is ferropericlas, CaPv is calcium perovskite, Bm is bridgmanite, and TaC is tantalum carbide.

tantalum carbide (TaC<sub>0.99</sub>) and constrained the pressure–volume–temperature equation of state (EOS).<sup>51</sup> The starting material was TaC<sub>0.99</sub> powder, and the pressure was determined by a thin piece of Au foil (less than 5  $\mu\text{m}$ ) using a published EOS.<sup>52</sup> In the first run, we started heating when the pressure reached 2 GPa, increased the temperature to 673 K, and measured x-ray diffraction up to a final pressure of 33 GPa along the 673 K isotherm.<sup>52</sup> In the second run, we increased the temperature at a pressure of  $\sim 2$  GPa up to 1073 K, and we collected x-ray diffraction images up to a final pressure of  $\sim 38$  GPa along an isothermal path. The data collected under non-hydrostatic conditions were used to constrain the quasi-hydrostatic high temperature EOS by extracting the hydrostatic unit-cell parameter from the x-ray diffraction data.<sup>51</sup> In addition, these data will be used in a future study to determine the strength and activity of the slip systems of TaC<sub>0.99</sub> at simultaneous high pressure and temperature.

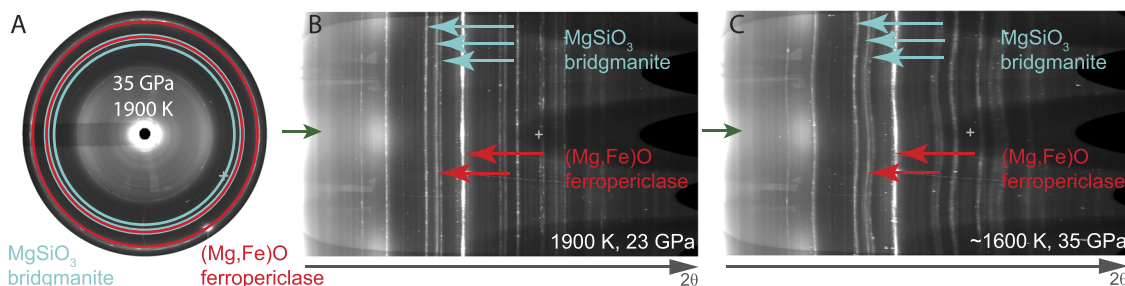


**FIG. 5.** Synthesis of bridgmanite (blue) + ferropericlas (red). Dark green arrows indicate the compression direction in the unrolled radial x-ray diffraction image. (a) Diffraction rings of bridgmanite and ferropericlas at 35 GPa and 1900 K. (b) Unrolled image with the straight unrolled diffraction rings of bridgmanite and ferropericlas at 23 GPa and 1900 K. (c) The unrolled diffraction image shows the curved diffraction rings of bridgmanite and ferropericlas after a pressure increase up to 35 GPa at  $\sim 1600$  K. Ferropericlas was used as the pressure calibrant.

### E. Challenges and solutions

In several experimental runs, the DAC jammed during high-temperature experiments, leading to discrete pressure jumps as opposed to smooth increases of pressure. Because of their brittleness, the ceramic gaskets were not able to buffer these pressure jumps, resulting in the failure of the diamond anvils. The reason for our difficulties to smoothly increase pressure at very high temperatures could be the expansion of both the piston and the cylinder of the Mao–Bell DAC, leading to increased friction between both parts. However, at moderately high temperatures, up to 1400 K, the differential cooling was effective such that a smooth pressure increase is generally possible. For higher temperature experiments, the indirect piston cooling is still insufficient and needs to be improved in order to reduce the thermal expansion of the piston and thus the friction.

Using the water-cooled vacuum chamber, temperatures up to 1900 K have been reached in the RH-rXRD-DAC, but no pressure increase was possible. Generally, both thermocouples recorded stable temperatures during the experiments, with a reproducible dependence of temperature on power (Fig. 6).

In a few runs, the difference in temperature reading between the two thermocouples was very large (the maximum difference observed was 400 K). In these cases, higher temperature values were recorded by the thermocouple situated between the graphite sheets. Large differences in temperature reading usually occurred when one of the thermocouples, i.e., the one at the tip of the diamond was placed too far from the culet of the diamond.

### IV. CONCLUSION

We have presented an improved experimental setup for radial x-ray diffraction measurements based on a graphite-heated

Mao–Bell type diamond-anvil cell contained in a water-cooled vacuum chamber. The setup is available for users at the Extreme Conditions Beamline P02.2 at DESY, Hamburg, and allows for reaching temperatures of up to 1900 K at high pressures (Fig. 7).

Temperature and pressure in the diamond-anvil cell are controlled remotely during the experiment. Several successful experimental studies were performed by using the improved setup on a variety of Earth materials (ferropericlase, calcium perovskite, and a two-phase bridgmanite–ferropericlase mixture) and tantalum carbide in order to show the capabilities of the resistive-heated-radial-x-ray-diffraction-diamond-anvil-cell. A major priority is currently the search for a better gasket material that combines large mechanical strength and high-temperature stability.

### ACKNOWLEDGMENTS

This research was supported through the German Science Foundation (Grant Nos. MA4534/3-1 and MA4534/4-1). H.M. acknowledges support from the Bavarian Academy of Sciences. L.M. acknowledges support from the U.S. Department of Energy, National Nuclear Security Administration, through the Capital-DOE Alliance Center (Grant No. DE-NA0003858) and NSF (Grant Nos. EAR-1344579 and EAR-1654687). S.M. acknowledges support from the Institut Universitaire de France and the program PNP of CNRS/INSU. We acknowledge DESY (Hamburg, Germany), a member of the Helmholtz Association HGF, for the provision of experimental facilities. Part of this research were supported by the Extreme Conditions Science Infrastructure (ECSI) at PETRA III, and we would like to thank K. Glazyrin for assistance in using Beamline P02.2. Part of the research leading to this result was supported by the project CALIPSO plus under the Grant Agreement No. 730872 from the EU Framework Programme for Research and Innovation HORIZON 2020.

### REFERENCES

- <sup>1</sup>D. L. Kohlstedt, *Properties of Rocks and Minerals—Constitutive Equations, Rheological Behavior, and Viscosity of Rocks* (Elsevier B.V., 2007).
- <sup>2</sup>N. Tsujino, Y. Nishihara, D. Yamazaki, Y. Seto, Y. Higo, and E. Takahashi, *Nature* **539**, 81 (2016).
- <sup>3</sup>J. Girard, G. Amulele, R. Farla, A. Mohiuddin, and S. Karato, *Science* **351**, 144 (2016).
- <sup>4</sup>S. Karato and P. Wu, *Science* **260**, 771 (1993).
- <sup>5</sup>D. Yamazaki and S. Karato, *Am. Mineral.* **86**, 385 (2001).
- <sup>6</sup>B. Romanowicz and H.-R. Wenk, *Phys. Earth Planet. Inter.* **269**, 58 (2017).
- <sup>7</sup>P. J. Tackley, *Science* **288**, 2002 (2000).
- <sup>8</sup>S. Karato, *Phys. Earth Planet. Inter.* **51**, 107 (1988).
- <sup>9</sup>S. Karato, S. Zhang, and H.-R. Wenk, *Science* **270**, 458 (1995).
- <sup>10</sup>J. Immoor, H. Marquardt, L. Miyagi, F. Lin, S. Speziale, S. Merkel, J. Buchen, A. Kurnosov, and H.-P. Liermann, *Earth Planet. Sci. Lett.* **489**, 251 (2018).
- <sup>11</sup>N. Creasy, M. D. Long, and H. A. Ford, *J. Geophys. Res.: Solid Earth* **122**, 5243, <https://doi.org/10.1029/2016jb013901> (2017).
- <sup>12</sup>C. P. Conrad, M. D. Behn, and P. G. Silver, *J. Geophys. Res.: Solid Earth* **112**, 1, <https://doi.org/10.1029/2006jb004608> (2007).
- <sup>13</sup>A. Nowacki, A. M. Walker, J. Wookey, and J.-M. Kendall, *Geophys. J. Int.* **192**, 1085 (2013).
- <sup>14</sup>T. Kawazoe, N. Nishiyama, Y. Nishihara, T. Irifune, D. Suetsugu, C. Bina, T. Inoue, D. Wiens, and M. Jellinek, *Phys. Earth Planet. Inter.* **183**, 190 (2010).

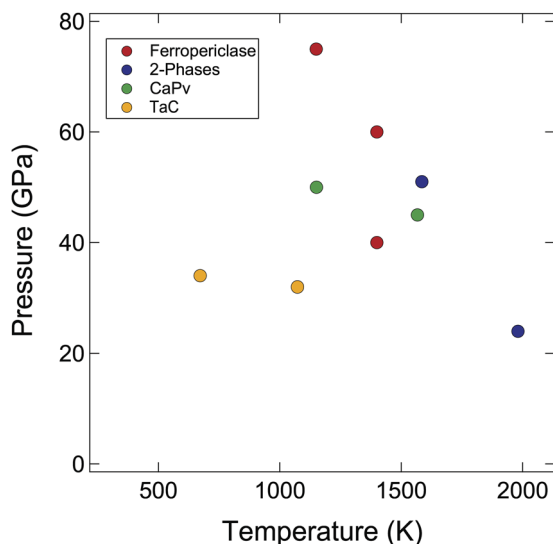


**FIG. 7.** Maximum pressure–temperature conditions reached in experiments on ferropericlase (red), 2-phases [enstatite (bridgmanite) + ferropericlase] (blue), calcium perovskite CaPv (green), and tantalum carbide TaC (yellow) in different experimental runs.

- <sup>15</sup>Y. Wang, W. B. Durham, I. C. Getting, and D. J. Weidner, *Rev. Sci. Instrum.* **74**, 3002 (2003).
- <sup>16</sup>D. Yamazaki and S.-I. Karato, *Rev. Sci. Instrum.* **72**, 4207 (2001).
- <sup>17</sup>T. Kawazoe, T. Ohuchi, Y. Nishihara, N. Nishiyama, K. Fujino, and T. Irifune, *Phys. Earth Planet. Inter.* **216**, 91 (2013).
- <sup>18</sup>S. A. Hunt and D. P. Dobson, *Rev. Sci. Instrum.* **88**, 126106 (2017).
- <sup>19</sup>H.-R. Wenk, I. Lonardelli, S. Merkel, L. Miyagi, J. Pehl, S. Speziale, and C. E. Tommaseo, *J. Phys.: Condens. Matter* **18**, S933 (2006).
- <sup>20</sup>S. Merkel, *J. Phys.: Condens. Matter* **18**, S949 (2006).
- <sup>21</sup>C. E. Tommaseo, J. Devine, S. Merkel, S. Speziale, and H.-R. Wenk, *Phys. Chem. Miner.* **33**, 84 (2006).
- <sup>22</sup>H. Marquardt and L. Miyagi, *Nat. Geosci.* **8**, 311 (2015).
- <sup>23</sup>L. Miyagi, S. Merkel, T. Yagi, N. Sata, Y. Ohishi, and H.-R. Wenk, *Phys. Earth Planet. Inter.* **174**, 159 (2009).
- <sup>24</sup>H.-R. Wenk, J. R. Baumgardner, R. A. Lebensohn, and C. N. Tomé, *J. Geophys. Res.: Solid Earth* **105**, 5663, <https://doi.org/10.1029/1999jb900346> (2000).
- <sup>25</sup>S. Merkel, A. K. McNamara, A. Kubo, S. Speziale, L. Miyagi, Y. Meng, T. S. Duffy, and H.-R. Wenk, *Science* **316**, 1729 (2007).
- <sup>26</sup>M. Kunz, W. A. Caldwell, L. Miyagi, and H.-R. Wenk, *Rev. Sci. Instrum.* **78**, 063907 (2007).
- <sup>27</sup>L. Miyagi, W. Kanitpanyacharoen, S. V. Raju, P. Kaercher, J. Knight, A. MacDowell, H.-R. Wenk, Q. Williams, and E. Z. Alarcon, *Rev. Sci. Instrum.* **84**, 025118 (2013).
- <sup>28</sup>H.-P. Liermann, S. Merkel, L. Miyagi, H.-R. Wenk, G. Shen, H. Cynn, and W. J. Evans, *Rev. Sci. Instrum.* **80**, 104501 (2009).
- <sup>29</sup>S. Merkel and T. Yagi, *Rev. Sci. Instrum.* **76**, 046109 (2005).
- <sup>30</sup>N. Funamori and T. Sato, *Rev. Sci. Instrum.* **79**, 053903 (2008).
- <sup>31</sup>H.-P. Liermann, Z. Konôpková, W. Morgenroth, K. Glazyrin, J. Bednarčík, E. McBride, S. Petitgirard, J. T. Delitz, M. Wendt, Y. Bican, A. Ehnes, I. Schwark, A. Rothkirch, M. Tischer, J. Heuer, H. Schulte-Schrepping, T. Kracht, and H. Franz, *J. Synchrotron Radiat.* **22**, 908 (2015).
- <sup>32</sup>S. Merkel, H.-P. Liermann, L. Miyagi, and H.-R. Wenk, *Acta Mater.* **61**, 5144 (2013).
- <sup>33</sup>H. Marquardt, S. Speziale, H. J. Reichmann, D. J. Frost, F. R. Schilling, and E. J. Garnero, *Science* **324**, 224 (2009).
- <sup>34</sup>J.-F. Lin, H.-R. Wenk, M. Voltolini, S. Speziale, J. Shu, and T. S. Duffy, *Phys. Chem. Miner.* **36**, 585 (2009).
- <sup>35</sup>S. Merkel, *J. Geophys. Res.* **107**, 2271, <https://doi.org/10.1029/2001JB000920> (2002).
- <sup>36</sup>D. Frost, *Elements* **4**, 171 (2008).
- <sup>37</sup>T. Irifune and T. Tsuchiya, *Treatise on Geophysics*, 2nd ed. (Elsevier B. V., Amsterdam, 2015).
- <sup>38</sup>K. Kawai and T. Tsuchiya, *Geophys. Res. Lett.* **42**, 2718, <https://doi.org/10.1002/2015gl063446> (2015).
- <sup>39</sup>S.-H. Shim, R. Jeanloz, and T. S. Duffy, *Geophys. Res. Lett.* **29**, 19, <https://doi.org/10.1029/2002gl016148> (2002).
- <sup>40</sup>R. Caracas, R. Wentzcovitch, G. D. Price, and J. Brodholt, *Geophys. Res. Lett.* **32**, L06306, <https://doi.org/10.1029/2004gl022144> (2005).
- <sup>41</sup>D. Y. Jung and A. R. Oganov, *Phys. Chem. Miner.* **32**, 146 (2005).
- <sup>42</sup>D. J. Adams and A. R. Oganov, *Phys. Rev. B* **73**, 184106 (2006).
- <sup>43</sup>T. Komabayashi, K. Hirose, N. Sata, Y. Ohishi, and L. S. Dubrovinsky, *Earth Planet. Sci. Lett.* **260**, 564 (2007).
- <sup>44</sup>T. Uchida, Y. Wang, N. Nishiyama, K.-I. Funakoshi, H. Kaneko, A. Nozawa, R. B. Von Dreele, M. L. Rivers, S. R. Sutton, A. Yamada, T. Kunitomo, T. Irifune, T. Inoue, and B. Li, *Earth Planet. Sci. Lett.* **282**, 268 (2009).
- <sup>45</sup>M. R. Handy, *J. Struct. Geol.* **16**, 287 (1994).
- <sup>46</sup>S. Karato, *Phys. Earth Planet. Inter.* **24**, 1 (1981).
- <sup>47</sup>Y.-T. Takeda, *J. Struct. Geol.* **20**, 1569 (1998).
- <sup>48</sup>M. Thielmann, G. J. Golabek, and H. Marquardt, *Geochem., Geophys., Geosyst.* **21**, 1, <https://doi.org/10.1029/2019gc008688> (2020).
- <sup>49</sup>Y. Wang, N. Hilaret, N. Nishiyama, N. Yahata, T. Tsuchiya, G. Morard, and G. Fiquet, *Geochem., Geophys., Geosyst.* **14**, 3389, <https://doi.org/10.1002/ggge.20200> (2013).
- <sup>50</sup>P. Kaercher, L. Miyagi, W. Kanitpanyacharoen, E. Zepeda-Alarcon, Y. Wang, F. De Carlo, and H. R. Wenk, *Earth Planet. Sci. Lett.* **456**, 134 (2016).
- <sup>51</sup>S. Speziale, J. Immoor, A. Ermakov, S. Merkel, H. Marquardt, and H.-P. Liermann, *J. Appl. Phys.* **126**, 105107 (2019).
- <sup>52</sup>Y. Fei, A. Ricolleau, M. Frank, K. Mibe, G. Shen, and V. Prakapenka, *Proc. Natl. Acad. Sci. U. S. A.* **104**, 9182 (2007).